Volume 16, Issue 4, 162504 (1-15)

International Journal of Industrial Chemistry (IJIC)

https://doi.org/10.57647/j.ijic.2025.1604.15

Development of a Hybrid α-Fe_2O_3-ZnO Photocatalyst Supported on Clinoptilolite for Pharmaceutical Pollutant Degradation

Mozhgan Zafari, Mohammad Reza Abedi*, Hassan Ali Zamani, Mahmoud Ebrahimi

Department of Applied Chemistry, Ma.C., Islamic Azad University, Mashhad, Iran

***Corresponding authors:** mohamadrezaabedi@iau.ac.ir

Article History:

Received:
23 October 2025

Revised:
30 November 2025

Accepted:
30 December 2025

Published in Issue:
30 December 2025

Abstract

Currently, it is well recognized that the protection and restoration of the fresh water sources is vital. In the current paper, α-Fe_2O_3/ZnO nanophotocatalysts supported on the surface of Clinoptilolite (CP) – (α-Fe_2O_3/ZnO/CP) using the solid-state dispersion (SSD) method was employed to degrade Atenolol (ATL) in aquatic environments. The UV/H_2O_2 process was used in this regard. All products were characterized by using FTIR, SEM, EDX and XRD. In order to reach optimal conditions, a full-factorial experimental design was used where the parameters affecting on the degradation including ATL concentration, catalyst loading, H_2O_2 concentration, pH, and catalyst composition were taken into account at three levels. ATL degradation was monitored using UV/VIS spectroscopy at λ = 224 nm. The final results indicated that the optimal conditions for reaching maximum degradation(x%=95.73) were as follows: ATL concentration = 10 mgL^{-1}, catalyst concentration = 300 mgL^{-1}, H_2O_2 concentration = 1 mgL^{-1}, pH = 9, chemical composition = Fe (75%), Zn (25%) and reaction time 75min. A first-order reaction with k = 0.0036 min^{-1} was observed for the photocatalytic degradation reaction.

Keywords: Atenolol; Clinoptilolite; α-Fe_2O_3; Full factorial; Photocatalyst; ZnO

Cite this article: Zafari M, Abedi M R, Zamani H A, Ebrahimi M. Development of a Hybrid α-Fe_2O_3-ZnO Photocatalyst Supported on Clinoptilolite for Pharmaceutical Pollutant Degradation. Int. J. Ind. Chem., 2025; 16(4):1-15. https://doi.org/10.57647/j.ijic.2025.1604.15

1. Introduction

In recent decades, development and activity in pharmaceutical industries and use of drugs by human societies caused to enter major parts of these drugs into the environment and water resources [1]. Removal of these types of chemical pollutants is very vital due to being valuable the fresh water.

The reports imply to presence of *β*-blockers in water resources [2-4]. ATL is one of the most widely consumed drugs of this family which its presence in water resources and wastewater from pharmaceutical industries has been reported [5, 6]. In order to eliminate and remove pharmaceutical pollutants, some different methods have been yet used which one of the most efficient methods is advanced oxidation processes (AOPs) [7]. Among various AOPs, there are some very common and effective photocatalytic processes where one or more photosensitive (photo-active) metal oxides were used as catalysts [8]. Decreased particle size of these catalysts to nanometer dimension could enhance their efficiency. In these processes, having illuminated the light on the nanophotocatalyst, electrons are promoted from the valence band (VB) to the conduction band (CB) and oxidation operation and degrading the molecular structure of the drug is done [9].

Various metal oxides are used as nanophotocatalyst which among them, Fe and Zn oxides are two common, effective and widely used ones [10, 11]. The concurrent use these two metal oxides and their utilization as nanophotocatalyst could be influential on the improved degradation efficiencies. Generally, nanophotocatalysts use could make some difficulties such as filtration after operation or their separation from the reactor.

Due to this, using the catalyst support will help to improve the process [12]. Different compounds are used as catalyst support which mineral compounds have special places among them. CP is a mineral compound with the formula of (NaKCa)2-3[$Al_3(AlSi)_2$ $Si_{13}O_{36}$].12H_2O which it can be used as catalyst support due to its high density and being water-insoluble [13]. The use of zeolites in nanophotocatalyst systems has significantly increased in recent years, with researchers extensively reviewing advancements in zeolite-based photocatalysis. Zeolites, with their unique properties like size, shape, and charge selectivity, are valuable components in developing modified nanophotocatalysts. These properties enable tailored interactions with reactants and light, leading to enhanced photocatalytic performance [14].

There are numerous procedures for synthesis of metal oxide nanoparticles (NPs) and their stabilization on the surface of catalyst support. Among these NPs synthesis procedures, techniques including co-precipitation, sol–gel, thermal degradation, Micelle, sonochemical synthesis, hydrothermal synthesis and forced hydrolysis and reflux condensation (FHRC) could be pointed out [15-20]. In order to stabilize the nanoparticles produced on the surface of catalyst support, the SSD method could be utilized. In this method, nanophotocatalyst precursor on the solid phase is mixed with catalyst support and then they are calcined [21]. After calcination, nanophotocatalyst precursor is both converted to metal oxide and chemically stabilized on the surface of catalyst support.

In the current paper, α-Fe_2O_3/ZnO nanocomposite supported on the surface of CP has been used for photocatalytic decomposition of ATL in aquatic environments. In order to optimize this process and study the effect of all parameters affecting on the degradation including concentration of the pollutant, catalyst concentration, H_2O_2 concentration, pH and catalyst composition are required to use Design of experiments (DOEs), because many parameters may have the interaction effects in addition to having direct effect on the response variable and therefore on the degradation efficiency [22].

In the paper, a full-factorial experimental design has been used for reaching optimal conditions and maximum degradation. Researchers have traditionally relied on the one-factor-at-a-time (OFAT) approach, where only one experimental variable is altered while all others remain constant. However, the design of experiments (DOE) methodology offers a more efficient alternative by allowing simultaneous variation of multiple factors. DOE is particularly advantageous when investigating interactions among two or more variables.

First, it requires fewer resources—including time, materials, and experimental runs—relative to the amount of data generated.

Second, DOE provides more accurate and robust estimates of individual factor effects, as a greater portion of the dataset contributes to the analysis, thereby reducing variability. In contrast, OFAT typically uses only a limited subset of observations to assess each factor's impact.

Third, DOE facilitates the evaluation of interactions between variables, a feature inherently absent in OFAT designs.

Finally, DOE enables exploration of system behavior across a broader experimental domain, offering a more comprehensive understanding of factor influences [23].

This study focuses on the synthesis and coupling of zinc oxide (ZnO) and α-iron(III) oxide (α-Fe_2O_3) nanoparticles to enhance their photocatalytic performance. ZnO is widely recognized as an efficient photocatalyst for environmental remediation; however, its practical application is limited by its poor absorption in the visible light region. On the other hand, α- Fe_2O_3 can absorb a broad range of visible light—up to 600 nm—covering more than 40% of the solar spectrum. Despite its advantages, including low cost and visible light activity, its photocatalytic performance is hindered by rapid electron–hole recombination, low electrical conductivity, and short hole diffusion lengths.

By coupling ZnO and α-Fe_2O_3, this research aims to synergistically enhance photocatalytic efficiency and address the intrinsic limitations of each individual material. Additionally, various modification techniques have been investigated to further improve the photocatalytic activities of these semiconductors [24].

Therefore, the main objectives of this study are as follows:

(1) to synthesize a ZnO/α-Fe_2O_3 nanocomposite supported on clinoptilolite (CP) using the solid-state dispersion (SSD) method;

(2) to evaluate its photocatalytic performance for the degradation of atenolol (ATL) under various operational conditions; and

(3) to optimize the degradation parameters—including pollutant concentration, catalyst dosage, pH, H_2O_2 concentration, and catalyst composition—using a full factorial design approach.

The study also aims to compare the efficiency of the proposed catalyst with previously reported photocatalytic systems and to provide insight into the synergistic effects

between ZnO and α-Fe_2O_3 in enhancing visible-light-driven photocatalysis.

2. Experimental

2.1. Materials and Methods

All chemical materials utilized for the current work include zinc nitrate hexahydrate ($Zn(NO_3)_2$. $6H_2O$), iron (III) chloride hexahydrate ($FeCl_3.6H_2O$), Urea (CH_4N_2O), sodium hydroxide (NaOH), hydrochloric acid (HCl, 37% pure), sulfuric acid (H_2SO_4, 96% pure), hydrogen peroxide (H_2O_2, 30% pure), ethanol (C_2H_5OH, 96% pure) which were purchased from Merck Co. (Germany) and they were used without any further purification. ATL was obtained from Tehran's Darou Pakhsh Co. (Iran) and a CP zeolite was prepared from Semnan minerals and mines development Co. (Iran). In order to wash the devices and solvation processes, deionized water was used. Fourier transform infrared (FTIR) spectra of products were recorded using an Alpha–Bruker FTIR spectrophotometer (TENSOR27, model) in the range of 500-3500 cm^{-1}. The shape, size and surface morphology of the prepared CP and α-Fe_2O_3/ZnO/CP were examined using the obtained images of a TESCAN MIRA III scanning electron microscope (SEM). The energy-dispersive X-ray (EDX) analysis was done using this device. The X-ray diffraction (XRD) analysis of the samples was carried out using a Philips PW1730 diffractometer. All UV/Vis absorption spectra were prepared using a Perkin-Elmer spectrophotometer (Lambda 950, model) and the pH values were determined by a Metrohm pH meter (model 827). In order to separate the catalyst from samples, an ALC 4232 centrifuge was utilized.

2.2. Synthesis of α-Fe_2O_3 Nanoparticles

For providing iron hydroxide ($Fe(OH)_3$) as a precursor for iron oxide according to Bharathi et al. [25], firstly, 100 ml $FeCl_3.6H_2O$ 0.25 M was poured into a flat-bottom flask and then 100 ml urea 1 M was gradually added to it during agitating. The obtained solution was stirred for 30 min and place under the reflex for 12 h at the temperature of 90-95°C. The precipitate obtained of the reflex was washed by deionized water several times until all unreacted materials will be removed. The precipitate was dried at 70°C inside an oven and after 2 h, a light brown solid was obtained. This solid was finally calcined in the furnace at 300°C for 1 h to transform the iron hydroxide to iron oxide.

2.3. Synthesis of ZnO Nanoparticles

In order to prepare Zinc hydroxide ($Zn(OH)_2$) as a precursor for Zinc oxide, based on the work of Getie et al. [26], firstly 12 g $Zn(NO_3)_2.6H_2O$ was dissolved in 100 ml distilled water and it was heated up at 75°C for 25 min, while moderately stirring. Then 3.2 g NaOH was dissolved in 30 ml distilled water and it was stirred for 10 min and finally, it was added to $Zn(NO_3)_2.6H_2O$ drop by drop. The yielded mixture was stirred under 70°C for 2 h. The generated solid was separated in the mixture by the filter paper and then it was calcined at 300°C for 1 h until Zinc will be transformed to Zinc oxide.

2.4. Preparation of α-Fe_2O_3/ZnO supported on the surface of CP using SSD method

The Solid-State Dispersion (SSD) method was employed for the fixation of the catalyst components onto the support material. This technique is favored due to its simplicity and potential for achieving uniform distribution, and it was utilized for the synthesis of **α**-Fe_2O_3/ZnO/CP catalyst. For the preparation of **α**-Fe_2O_3/ZnO/CP via the SSD route, the catalyst precursors (iron hydroxide and zinc hydroxide) and the CP support material were first prepared and purified separately.

2.4.1. *Optimization of the SSD Mixing Parameters and Precursor-to-Support Ratio*

To ensure reproducibility and uniform distribution of the precursor particles on the clinoptilolite surface, the mixing parameters in the SSD process were systematically optimized. Preliminary trials were conducted to determine the ideal solvent amount, mixing time, and precursor-to-support ratio. During the optimization, it was observed that achieving a controlled paste-like consistency was crucial for preventing particle agglomeration and ensuring homogeneous coating. For this purpose, ethanol was added only through micro-spray increments to maintain the mixture within a narrow viscosity range; excessive ethanol led to slurry dilution and uneven spreading, while insufficient ethanol caused premature hardening of the paste. Through these trials, a mixing duration of one hour was found to be optimal, as shorter times resulted in incomplete blending, whereas longer mixing did not yield additional benefits. The selected precursor-to-support ratio of 1:3 (total $Fe(OH)_3$ + $Zn(OH)_2$: CP) was also optimized through comparative experiments. Higher loadings (e.g., 1:1 or 1:2) caused excessive precursor aggregation and partial blockage of the CP micropores, reducing the effective surface area and limiting adsorption–photocatalysis synergy. In contrast, lower loadings (e.g., 1:4 or 1:5) produced highly uniform coatings but insufficient active sites for efficient photocatalysis. The 1:3 ratio was therefore identified as the optimal compromise, providing (i) adequate active phase deposition, (ii) minimal pore obstruction, (iii)

preservation of the structural and adsorption properties of clinoptilolite, and (iv) robust anchoring of the oxide nanoparticles during calcination. These optimized parameters ensured consistent SSD performance and reproducible catalyst preparation.

2.4.2. *Drying and Calcination Stages*

Improper addition of ethanol or failure to maintain the paste consistency during the process can lead to mixing issues and product agglomeration. After successful mixing, the resulting paste was exposed to ambient air for one hour to allow for the evaporation of the bulk surface ethanol. Subsequently, for complete drying, the mixture was transferred to an oven and dried at a controlled temperature of 80°C for one hour.

Finally, for calcination and the thermal conversion of the deposited iron and zinc hydroxides into iron oxide(α-Fe_2O_3) and zinc oxide (ZnO), the dried mixture was heated in a furnace at 300 °C for one hour (under air atmosphere). This thermal fixation process successfully anchored the α-Fe_2O_3 and ZnO particles onto the CP support using the SSD method.

2.5. Full-Factorial Experimental Design

Analysis of variance (ANOVA) is a statistical method for making simultaneous comparisons and analyze the differences between group means and associated procedures. ANOVAs function for examining two, three or more means of variables from statistical significance viewpoint. ANOVA was utilized for graphical analyses of the data in order to get the interaction effect among the process factors and the responses.

The quality of the fit polynomial model was expressed by the coefficient of determination or R^2, and its statistical significance was checked by the Fisher's F test in the same program. Model terms were evaluated by the P-value. In Table 3, the estimated effects and coefficients for x% have been provided. In this table, standard deviation (S), correlation coefficient, predicted R-squared (pred. R^2) and adjusted R-squared (adj R^2) values were also reported. The square of the correlation coefficient for each response was calculated as the coefficient of determination (R^2).

The ANOVA results demonstrated that all main factors and their interactions significantly affected the ATL degradation ($p < 0.05$), except the center point ($p = 0.141$), which indicates the adequacy of the quadratic model and the absence of curvature in the response surface.

The 95% confidence intervals of the estimated coefficients confirmed their statistical reliability. The high R^2 (99.78%), adjusted R^2 (99.42%), and predicted R^2 (98.23%) values further verified the excellent fitting and prediction capability of the model. All analyses were carried out at a 95% confidence level using Minitab 16.2.0.

The Full-Factorial Design of Experiments provided a statistically valid and reliable model (supported by p-values and Confidence Intervals**)** that identified the crucial direct and interactive effects of the five process variables. The optimal degradation efficiency for Atenolol (ATL) was achieved under conditions of pH=9, low initial ATL concentration (10 mgL^{-1}), high H_2O_2 concentration (4 mgL^{-1}), catalyst composition of 75% Fe / 25% Zn and reaction time 75min.

The statistical significance of both the main factors and their interaction terms was further evaluated through the p-values obtained from the ANOVA analysis. In this study, all model terms with $p < 0.05$ were considered statistically significant, indicating that these variables exert a real and measurable effect on the photodegradation efficiency of Atenolol. The low p-values of several interaction terms—such as Initial concentration × Catalyst concentration, H_2O_2 concentration × pH, and Initial concentration × Catalyst composition—demonstrate that the combined influence of these parameters is more important than their individual contributions. This confirms that the syste++m demonstrates true interaction behavior, which justifies the use of a full-factorial rather than an OFAT design.

Furthermore, the narrow 95% confidence intervals of the estimated coefficients indicate a high level of reliability and precision in the model predictions. The excellent agreement between R^2 (99.78%), adjusted R^2 (99.42%), and predicted R^2 (98.23%) confirms that the model is neither overfitted nor underfitted, and accurately reflects the experimental domain. These statistical indicators collectively validate the robustness and predictive capability of the developed factorial model

The nanophotocatalytic efficiency of α-Fe_2O_3/ZnO/CP on the ATL degradation was examined using DoE. The experiments were designed considering five variables affecting on the process including pH, ATL concentration, catalyst concentration, catalyst composition and H_2O_2 concentration at three levels(-1, 0 and +1).

Experimental ranges and levels of any variable are listed in Table 1. pH was varied from 5 to 9 at three levels (5, 7 and 9), initial concentration of ATL from 10 to 50 at three levels (10, 30 and 50(mgL^{-1})), catalyst concentration from 300 to 600 at three levels (300, 450 and 600(mgL^{-1})) and H_2O_2 concentration from 2 to 4 at three levels (2, 3 and 4(mgL^{-1})).

In table 2, 35 experiments relevant to this experimental design and conditions of any variable has been reported. In order to carry out DoE, Minitab version 16.2.0 was utilized as statistical software. Moreover, analysis of variance (ANOVA) was run to analyze the results.

Table 1. Experimental conditions for photocatalytic degradation of ATL

RunOrder	Catalyst Con. (mgL^{-1})	Initial Con. of ATL (mgL^{-1})	H_2O_2 Con. (mgL^{-1})	pH	Catalyst Com. (Fe/Zn %) (w/w)
1	450	30	3	7	50/50
2	300	10	4	9	75/25
3	600	10	4	5	75/25
4	600	10	4	9	75/25
5	300	50	4	9	75/25
6	600	50	2	9	25/75
7	600	50	2	5	25/75
8	600	50	4	9	25/75
9	300	50	2	9	75/25
10	300	10	4	9	25/75
11	300	10	4	5	25/75
12	300	10	2	5	25/75
13	600	10	4	9	25/75
14	300	50	4	5	25/75
15	600	10	4	5	25/75
16	600	10	2	9	75/25
17	450	30	3	7	50/50
18	300	50	2	5	75/25
19	450	30	3	7	50/50
20	600	50	2	5	75/25
21	300	10	4	5	75/25
22	600	50	2	9	75/25
23	300	10	2	9	25/75
24	300	50	2	9	25/75
25	600	10	2	9	25/75
26	600	50	4	5	25/75
27	600	50	4	5	75/25
28	600	10	2	5	75/25
29	600	10	2	5	25/75
30	300	50	4	5	75/25
31	300	50	4	9	25/75
32	600	50	4	9	75/25
33	300	50	2	5	25/75
34	300	50	2	9	75/25
35	300	10	2	5	75/25

2.6. Photocatalytic degradation process

In order to do experimental operations, an MDF box with size of 70 × 70 × 70 cm equipped with an air-conditioning system was utilized. The reactor was a Pyrex glass dish with 500 ml capacity and was placed at a distance of 7 cm from UV lamps. In this process, two UV 15 W lamps were used. The solution inside the reactor was continuously agitated and sampling was performed by a 5 ml syringe. For performing each experiment, 500 ml ATL with specific concentration and pH was poured into the reactor. pH was adjusted using two solutions NaOH and H_2SO_4. At that time based on the conditions of each experiment (specified in table 1), specific amount of H_2O_2 and catalyst were added to the reactor and at the same time, UV lamps were turned on.

The beginning of the reaction time was calculated from the moment of turning on the UV lamps and adding the materials into the reactor; samplings were run every 25 min. In order to separate the catalyst from aqueous solution, the samples were centrifuged for 5 min with 3500 rpm speed. After degradation process, the ATL concentration of the samples were calculated based on the equation of Beer-Lambert law (equ. 1) at λmax 224 nm.

$$A = \varepsilon bC \quad (1)$$

Where A corresponds the absorbance, ε is the absorptivity coefficient, b is the cell length and C corresponds to the concentration of analyte.

The percent of photodegradation efficiency (x%) is shown as a function of time is given by:

$$x\% = \frac{C_0 - C}{C_0} \times 100 \quad (2)$$

In the above equation, C0 and C are the concentration of ATL at t = 0 and t, respectively.

3. Results and Discussion

The SEM images related to CP catalyst support and α-Fe_2O_3/ZnO/CP catalyst have been shown in fig. 1a and 1b respectively. SEM micrographs revealed a uniform dispersion of nearly spherical α-Fe_2O_3 particles and rod-like ZnO structures on the clinoptilolite surface. The CP substrate exhibited a rough and porous morphology, which facilitated the immobilization and spatial separation of the nanoparticles. This heterogeneous surface topography enhances light scattering and provides more active sites for photocatalytic reactions. Agglomeration was minimal, indicating effective dispersion and anchoring achieved by the SSD synthesis approach. In fig. 2, the results of EDX related to α-Fe_2O_3/ZnO/CP have been shown. Furthermore, the EDX spectrum confirmed the elemental composition of Fe, Zn, O, Si, and Al, verifying the coexistence of the oxides with the CP support. The quantitative atomic ratios obtained from EDX analysis were consistent with the nominal Fe/Zn ratio used during synthesis, demonstrating the reliability of the loading process. The absence of extraneous elemental peaks further supports the chemical purity of the prepared catalyst.

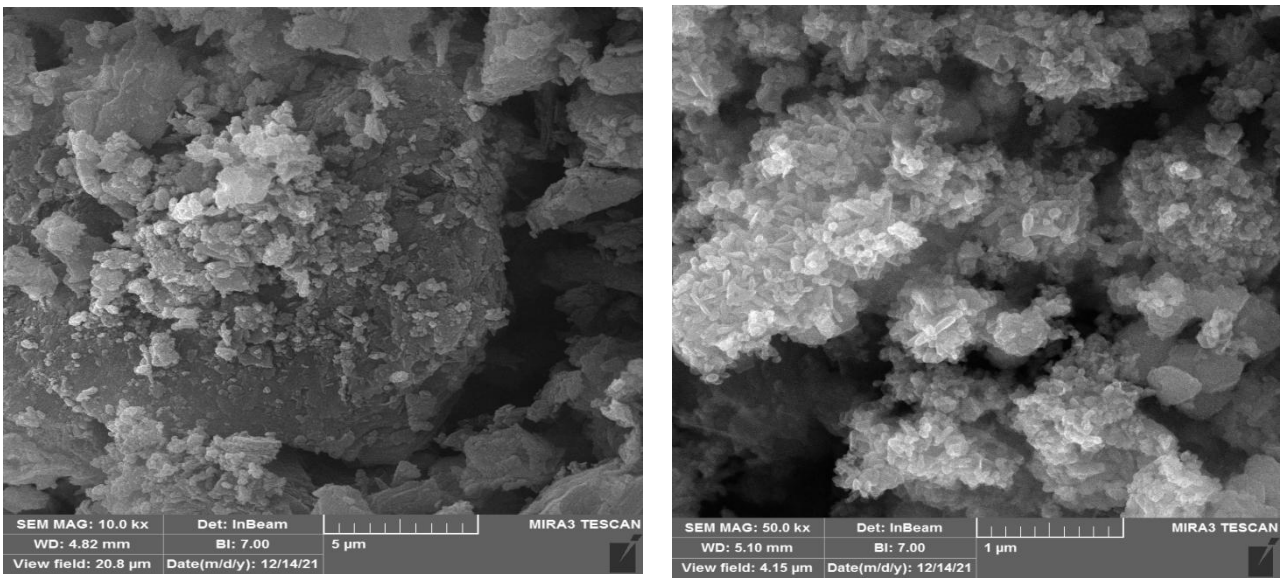

(a) (b)

Figure 1. (a) CP catalyst support; (b) α-Fe_2O_3/ZnO/CP catalyst

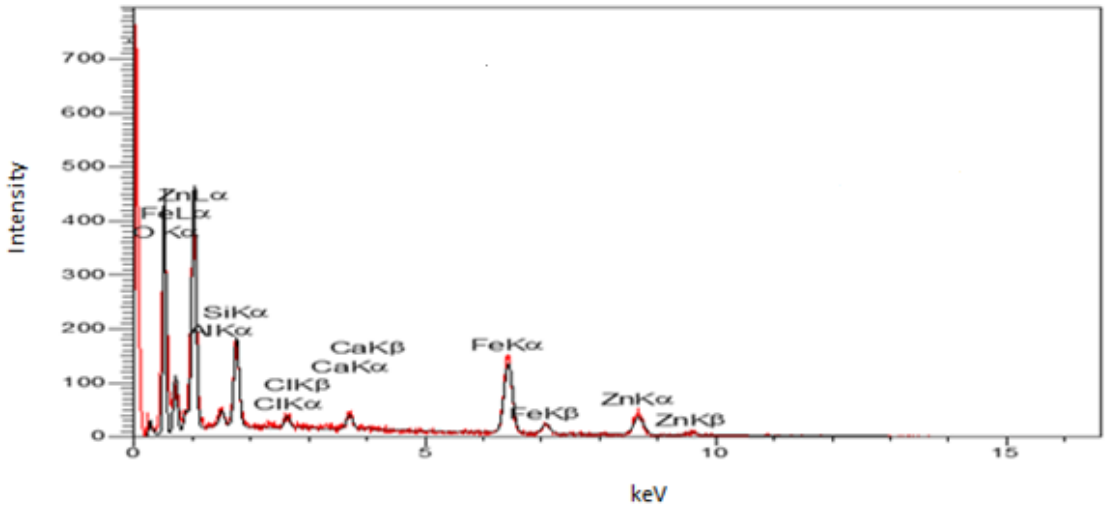

Figure 2. The results of EDX analysis related to α-Fe_2O_3/ZnO/CP

In Fig. 3b the observed peaks located at 468.44, 561.79, 795.17, 1064, 1636.46 and 3429.69 cm^{-1} are in agreement with IR spectral data reported for clinoptilolite [27]. In fig. 3 (b), FTIR spectra analysis related to catalyst support of CP has been shown where the most intensive absorption band is located at 1064 cm^{-1}. This absorption peak corresponds to the stretching vibration of Si(Al)-O in the $Si(Al)O_4$ tetrahedral atoms which it kept unchanged location after incorporation with α-Fe_2O_3/ZnO and it has not been shifted. In fig. 3 (a), the absorption peak appeared at 468 cm^{-1} belongs to ZnO and the one appeared at 561 cm^{-1} belongs to Fe_2O_3. Fig. 4 (a) and (b) show the XRD pattern of α-Fe_2O_3/ZnO/CP catalyst and CP, respectively. As it can be seen that in the XRD pattern of α-Fe_2O_3/ZnO/CP, all the characteristic peaks corresponded to CP (appeared in the b pattern) are well appeared but only their intensities have been reduced to a slight extent. This means that during supporting processes, catalyst support has not been chemically and structurally changed, only its surface has been covered with α-Fe_2O_3 and ZnO. Appearance of characteristic peaks of α-Fe_2O_3/ZnO in XRD pattern is in the agreement with results of Bharati et al. which confirms the successful synthesizing and stabilizing Iron/Zinc oxides. The XRD pattern related to α-Fe_2O_3/ZnO/CP using Warren–Averbach theory and calculating and taking account of the device errors indicated that average crystallite size of this catalyst is 84.53 nm [28].

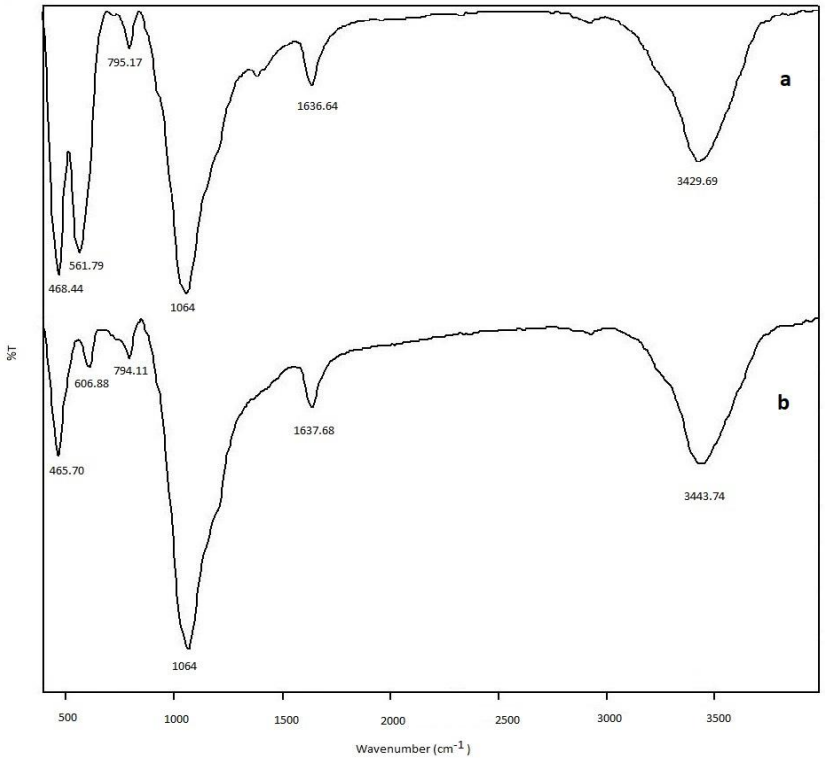

Figure 3. FTIR spectra of (a) α-Fe_2O_3/ZnO/CP and (b) CP

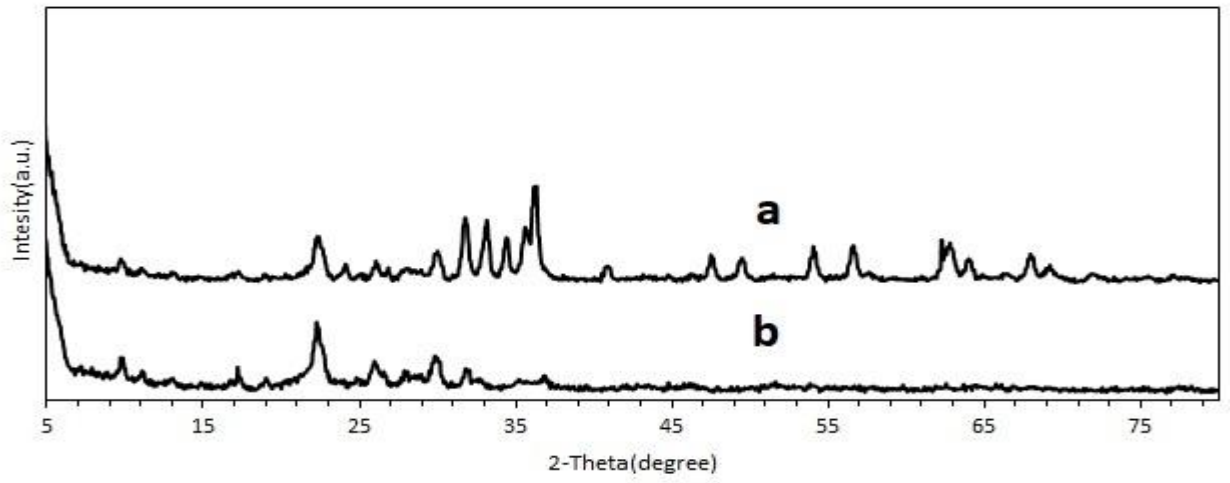

Figure 4. XRD related to α-Fe_2O_3/ZnO/CP catalyst (a) and CP (b)

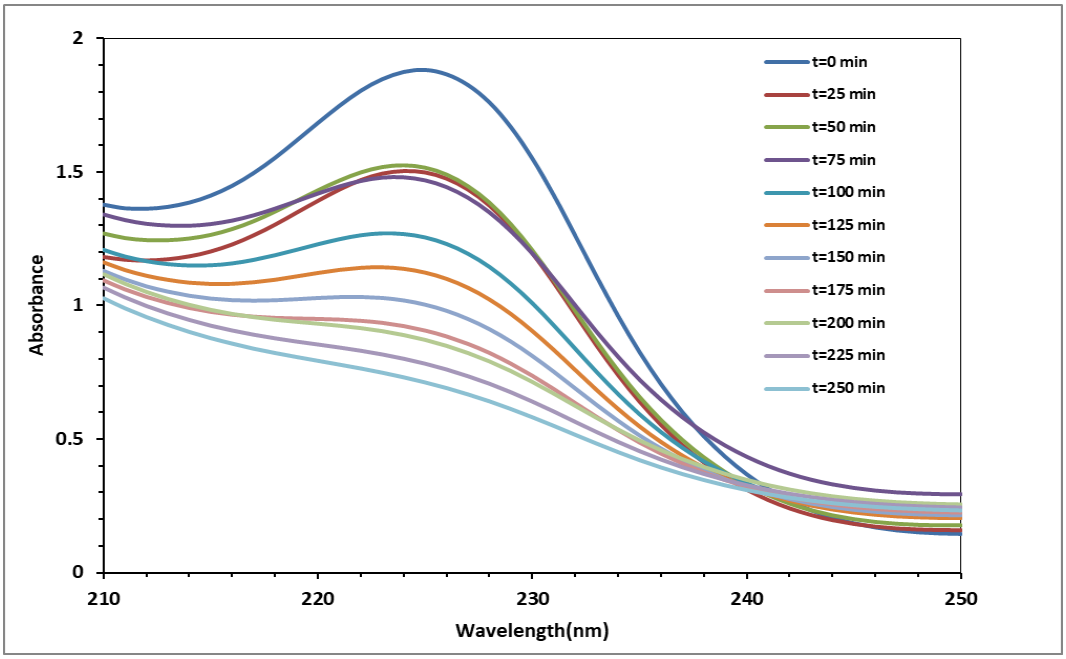

Figure 5. UV/Vis spectral absorption changes of ATL degraded by α-Fe_2O_3/ZnO/CP related to the experiment No. 33

The combined results from FTIR, XRD, SEM, and EDX analyses coherently substantiate the successful formation of a structurally stable α-Fe_2O_3/ZnO/CP nanocomposite with intimate interfacial contact between the two semiconductor phases. This configuration facilitates efficient charge separation and transfer between ZnO and Fe_2O_3, minimizing electron–hole recombination and thereby accounting for the superior photocatalytic degradation of Atenolol (ATL) observed in the study. The porosity and large surface area of the CP support, confirmed by morphological evidence, further contribute to enhanced adsorption–photocatalysis synergy. Accordingly, the characterization results provide both structural and mechanistic validation for the improved efficiency and stability claims made for the α-Fe_2O_3/ZnO/CP composite photocatalyst.

3.1. UV/Vis Spectra Kinetics of photocatalytic degradation of ATL

Fig. 5 shows the absorption spectra based on the wavelength for degradation process of ATL at the beginning of reaction (t = 0) and following 25, 50, 75, 100, 125, 150, 175, 200, 225 and 250 min after reaction. In order to determine the concentration of ATL at any interval, Equ. 1 was used and Equ. 2 (taking account the absorption at λ_{max} = 224 nm) was employed to calculate the % x. [29].

3.2. Degradation mechanism

Based on the obtained results, a possible mechanism for the degradation of ATL using the α-Fe_2O_3/ZnO/CP photocatalyst is proposed. During the photocatalytic process, photon absorption by the α- Fe_2O_3/ZnO semiconductor composite promotes electrons from the valence band (VB) to the conduction band (CB), resulting in the generation of electron–hole pairs (Eq. (3)). These charge carriers are susceptible to recombination, which can reduce photocatalytic efficiency (Eq. (4)). Notably, the pre-adsorption of the ATL substrate onto the photocatalyst surface has been reported as a crucial step for achieving high degradation efficiency. The photogenerated holes in the valence band of α- Fe_2O_3/ZnO can oxidize adsorbed water molecules or hydroxide ions to generate hydroxyl radicals (•OH), which are strong oxidizing species responsible for pollutant degradation (Eqs. (5) and (6)) [30].

$$\alpha - Fe_2O_3/ZnO + h\nu \rightarrow \alpha\text{–}Fe_2O_3/ZnO(e^-_{CB} + h^+_{VB}) \quad (3)$$

$$e^-_{CB} + h^+_{VB} \rightarrow \text{heat} \quad (4)$$

$$h^+_{VB} + H_2O_{(ads)} \rightarrow {}^\circ OH_{(ads)} + H^+ \quad (5)$$

$$h^+_{VB} + OH^-_{ads} \rightarrow {}^\circ OH_{(ads)} \quad (6)$$

The photo-generated electrons in the conduction band can react with dissolved molecular oxygen, leading to the formation of superoxide anion radicals (•O_2^-) (Eq. (7)). In the presence of organic scavengers, these reactive oxygen species may subsequently participate in the formation of organic peroxides or hydrogen peroxide (Eqs. (8) and (9)). The hydroxyl radical (•OH), recognized as a highly potent oxidizing species, can aggressively attack organic

pollutants, resulting in the formation of intermediate compounds (Int.) [31]. These intermediates further undergo oxidation by hydroxyl radicals, eventually converting into stable final products (P), such as carbon dioxide and water (Eq. (10)).

$$e_{CB}^{-} + O_{2(ads)} \rightarrow {}^{\circ}O_{2(ads)}^{-} \quad (7)$$

$${}^{\circ}O_{2(ads)}^{-} + H_2O^{\circ} + H^{+} \rightarrow H_2O_2 + O_2 \quad (8)$$

$${}^{\circ}O_{2(ads)}^{-} + ATL \rightarrow ATL - OO^{\circ} \quad (9)$$

$${}^{\circ}OH_{(ads)} + \mathrm{ATL} \rightarrow \mathrm{Int.} \rightarrow \mathrm{P} \quad (10)$$

Recent studies have demonstrated that several reactive oxygen species (ROS) contribute synergistically to the photocatalytic degradation of β-blocker pharmaceuticals. In the α-Fe_2O_3/ZnO heterojunction system, hydroxyl radicals (•OH) are the dominant oxidizing species due to the strong oxidation potential of photogenerated holes. Superoxide radicals (•O_2^-) also play an important role by initiating secondary oxidation reactions and producing hydroperoxyl radicals (HO_2•), which subsequently decompose to form additional •OH through H_2O_2 intermediates. The presence of α-Fe_2O_3 enhances visible-light absorption and promotes charge separation, while ZnO facilitates rapid electron transfer to dissolved oxygen, accelerating •O_2^- formation. Together, these ROS species attack the aromatic rings and ether bonds of Atenolol, leading to rapid fragmentation and mineralization. These mechanistic steps are consistent with recent reports on ROS-driven degradation pathways of pharmaceutical contaminants

3.3. Kinetics of photocatalytic degradation of ATL

Fig. 6 shows the plot of ln(C0/C) versus time. The linearity of the plot suggests that the ATL photodegradation reaction follows first-order kinetics. The degradation reaction of ATL was investigated in terms of reaction order kinetics. Based on the results obtained in Table 2, the reaction was found to follow first-order kinetics.

Although the degradation of Atenolol follows a first-order kinetic model with the highest R^2 value (0.99), the comparison with zero- and second-order models provides useful insight into the reaction pathway. The inferior fit of the zero-order model suggests that the degradation is not limited by photon flux alone, while the relatively high but lower R^2 for the second-order model indicates that bimolecular interactions between surface-adsorbed species are less dominant.

The strong agreement with first-order behavior is consistent with surface-controlled photocatalytic reactions in which the concentration of organic pollutant decreases exponentially due to continuous ROS attack on adsorbed molecules. These observations support the proposed mechanism and validate the kinetic interpretation.

3.4. Optimal conditions

3.4.1. *ANOVA and fit summary*

The accuracy and variability of the model can be estimated by R^2. The R^2 value is always between 0 and 1. The closer the R^2 value to 1, the stronger the model is and the better the model predicts the response (x%). In this paper, R^2 value was reported to be 99.78. The ‘‘pred R^2 ’’ of 98.23 is in reasonable agreement with the ‘‘adj R^2 ’’ of 99.42, confirming good predictability of the model.

Table 2. Kinetic models adjustment for ATL

	Zero-order		First-order		Second-order	
	$C\text{-}C_0 = -kt$		$Ln(C/C_0) = kt$		$1/C - 1/C_0 = kt$	
pH	k	R^2	k	R^2	k	R^2
5	-0.0042	0.98	0.0036	0.99	0.0032	0.98

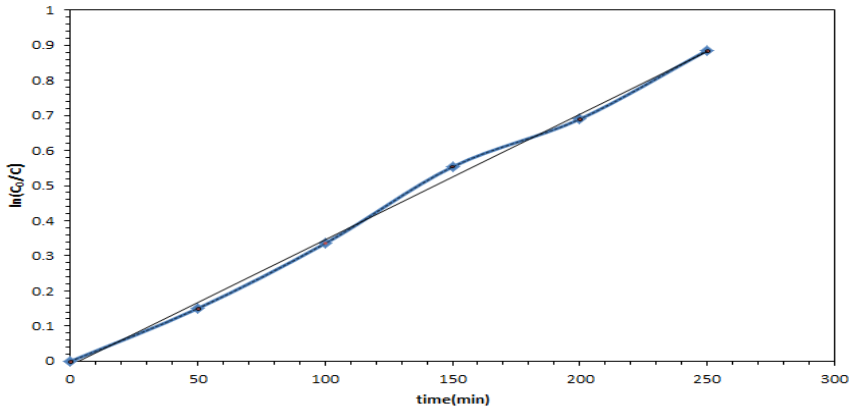

Figure 6. Plot of chemical first-order kinetics: The initial concentration of ATL = 50 mgL^{-1}, catalyst concentration = 300 mgL^{-1}, H_2O_2 concentration = 2 mgL^{-1} and pH = 5

Table 3. The estimated effects and coefficients for photodegradation efficiency (x%)

Term	Effect	Coef.	SE Coef.	T-Value	P-Value	VIF	Result
Constant	-	36.889	0.234	157.84	0.000		
Catalyst con.	1.434	0.717	0.234	3.07	0.009	1.00	
Initial con. of ATL	-19.230	-9.615	0.234	-41.14	0.000	1.00	
H_2O_2 con.	13.509	6.754	0.234	28.90	0.003	1.00	
pH	-1.702	-0.851	0.234	-3.64	0.000	1.00	
Catalyst Comp.	11.288	5.644	0.234	24.15	0.000	1.00	
Catalyst con.* Initial con.of ATL	5.432	2.716	0.234	11.62	0.000	1.00	
Catalyst con.* H_2O_2 con.	-7.914	-3.957	0.234	-16.93	0.000	1.00	
Catalyst con.*pH	-8.520	-4.260	0.234	-18.23	0.000	1.00	
Catalyst con.* Catalyst Comp.	2.890	1.445	0.234	6.18	0.000	1.00	
Initial con.of ATL * H_2O_2 con.	-11.418	-5.709	0.234	-24.43	0.000	1.00	
Initial con.of ATL *pH	-4.286	-2.143	0.234	-9.17	0.000	1.00	
Initial con.of ATL * Catalyst Comp.	-9.151	-4.576	0.234	-19.58	0.000	1.00	
H_2O_2 con.*pH	9.560	4.780	0.234	20.45	0.000	1.00	
H_2O_2 con.* Catalyst Comp.	5.587	2.794	0.234	11.95	0.000	1.00	
pH* Catalyst Comp.	1.011	0.506	0.234	2.16	0.000	1.00	
Center Point	-	-1.253	0.798	-1.57	0.141	1.00	

S = 1.32211, R^2 = 99.78% , pred R^2 = 98.22%, Adj R^2 = 99.42%

Based on table 3 and the significant variables effects on the response, magnitudes of effects for the initial concentration of ATL, pH, H_2O_2 concentration, catalyst concentration and catalyst composition are as 19.230, 1.702, 13.509, 1.434 and 11.288, respectively. Thus, the significant reaction parameters were (the greatest to the least significant): initial concentration of ATL > H_2O_2 concentration > catalyst composition > pH > catalyst concentration [32].

3.4.2. *Diagnostics plots*

It is necessary to note that the parameters of initial concentration and pH negatively affect on the response (-19.230 and 1.702). It means that increasing the initial concentration of ATL and pH causes to decrease photodegradation efficiency (x%) and reduction of these two factors will increase the photodegradation efficiency (x%). But the parameters of H_2O_2 concentration and catalyst composition have a positive effect on the response factor and increasing these parameters will be caused to enhance the photodegradation efficiency (x%).

Based on the table 3, it could be seen that interaction effects between the initial concentration of ATL and catalyst concentration is 5.432, between the type of catalyst and catalyst concentration as 2.890, between H_2O_2 concentration and pH as 9.560, between H_2O_2 concentration and the type of catalyst as 5.587 and between type of the catalyst and pH as 1.011. It is essential to note that P-values have been examined using an alpha (α) level of 0.05.

In order to compare the effect of variables on the response, the fig. 7a could be used which is a Pareto plot of the standardized effects. In this figure, those variables whose effects on the response is negative (-) or positive (+), have been marked.

In this plot, it is clear that the effect of the initial concentration of ATL on the photodegradation efficiency (x%) is greater than other parameters, but the effect of this variable is negative. It means that increasing or decreasing the initial concentration of ATL are caused to decrease or increase the photodegradation efficiency (x%), respectively.

In order to better investigate the residual values, residual plot versus experiment No. has been illustrated in fig. 7b. As it can be seen that 16 points are located above zero lines (positive), 15 residual points under zero lines (negative) and 4 points on the zero line. Owing to this observation and comparison of distance between these points and zero lines, it could be said that the residuals are normally distributed.

A highly useful procedure is to draw a normal probability residuals plot. If the underlying residuals distribution is normal, this plot will be similar to a straight line.

Fig. 7c shows normal probability plot. In this plot, it is evident that residuals distribution is normal because points (especially central points) are near straight line. If the model is correct and if the assumptions are satisfied, the residuals should not have structure; in particular, they should be unrelated to any other variable including the predicted response.

A simple check is to plot the residuals versus the fitted values. Fig. 7d shows plot of residuals versus fitted values. Mathematical model representing ATL photocatalytic degradation in the range studied can be expressed by the following equation:

Response = % x

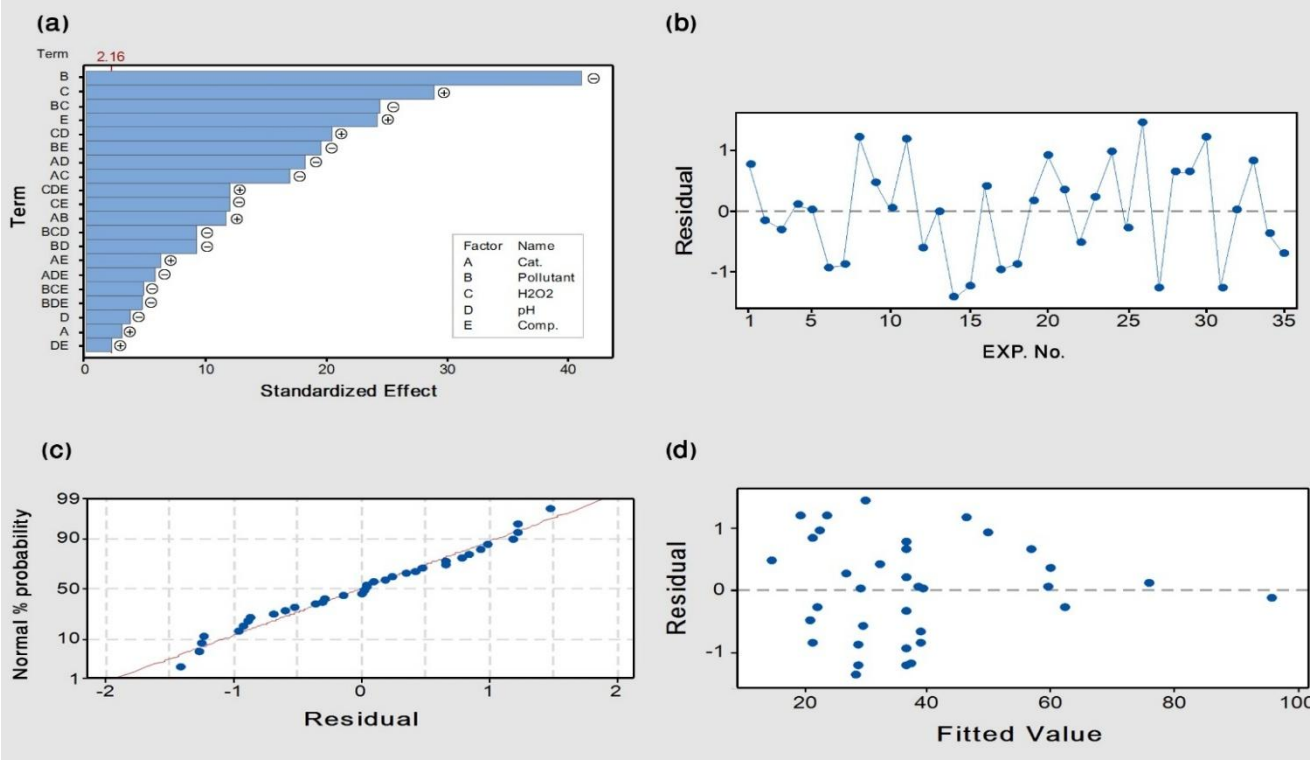

Figure 7. (a). The pareto chart of the standardized effects, (b) plot of residuals versus experiment No., (c) Normal probability plot, (d) plot of residuals versus fitted values related to photocatalytic degradation of atenolol (ATL) using the catalyst prepared through the SSD method

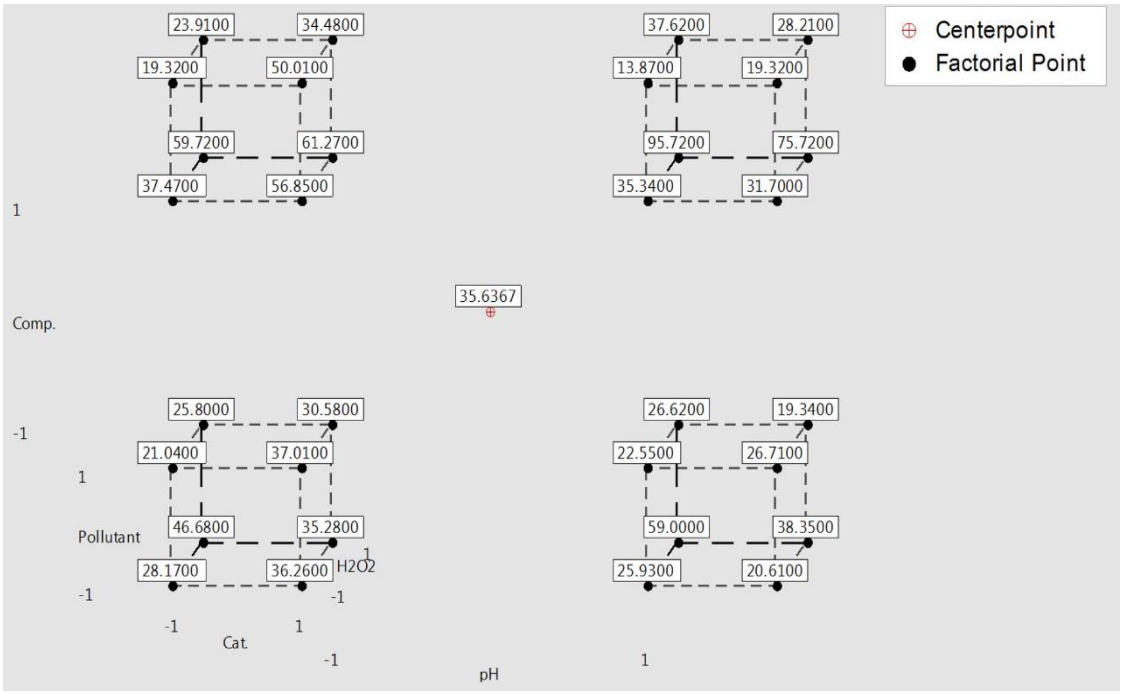

Figure 8. The cube plot for x%

= 36.889 + 0.717 A - 9.615 B+ 6.754 C - 0.851 D
+ 5.644 E + 2.716 A*B - 3.957 A*C - 4.260 A*D
+ 1.445 A*E - 5.709 B*C - 2.143 B*D - 4.576 B*E
+ 4.780 C*D + 2.794 C*E + 0.506 D*E -…

Where A, B, C, D and E are catalyst concentration, the initial concentration of ATL, H_2O_2 concentration and catalyst composition, respectively.

3.4.3. *Cube Plot Analysis*

The cube plot for x% is shown in fig. 8. Using this cube plot, the condition for reaching the desirable response (x%) could be easily identified. For instance, in order to reach maximum degradation (x% = 95.73), respectively. The initial concentration of ATL, pH, H_2O_2 concentration, catalyst concentration and catalyst composition should be

at levels of -1 (10 mgL^{-1}), +1 (9), +1 (4 mgL^{-1}), -1 (300 mgL^{-1}) and +1 (Fe(75%)-Zn(25%)), respectively. Generally, the interaction effects are vital and they affect on the response, because they may place unpredictable effects on the response.

For example, based on fig. 8, despite the fact that factors of catalyst and pH have positive effects but with low magnitude on the response, while they place interaction effect on each other, their effects on the response (x%) will become more [33].

3.5. Comparison with other photocatalysts

The photocatalytic performance of the materials synthesized in this study was evaluated for the degradation of ATL and compared to recently reported photocatalysts (Table 4). The data reveal a significant enhancement in the degradation percentage of AT using the newly prepared photocatalysts, suggesting a superior ability to generate electron-hole pairs compared to previously studied materials.

Furthermore, the degradation time required for AT was considerably reduced, indicating faster reaction kinetics. These findings underscore the improved efficiency of the novel photocatalytic materials in facilitating the degradation of these pharmaceuticals, highlighting their potential for more effective water purification applications.

The performance of the α-Fe_2O_3/ZnO/CP photocatalyst demonstrates several advantages over previously reported systems. The strong interfacial contact between α-Fe_2O_3 and ZnO reduces electron–hole recombination, enabling a shorter degradation time compared to TiO_2-based and Ag-modified photocatalysts. The use of natural clinoptilolite as a support also provides a low-cost and environmentally benign alternative with improved separation and recyclability.

However, similar to other advanced oxidation processes, the present system requires the presence of H_2O_2 as an external oxidant, which may increase operational costs in large-scale applications. From a scalability perspective, the solid-state dispersion (SSD) synthesis route and the abundance of clinoptilolite suggest that the proposed material can be readily produced in higher quantities and integrated into continuous-flow photoreactors for industrial wastewater treatment.

3.6. Environmental Considerations

Although the photocatalytic degradation of Atenolol proceeds efficiently using the α-Fe_2O_3/ZnO/CP system, the environmental impact of intermediate byproducts must also be considered. Previous reports have shown that certain β-blocker degradation intermediates may exhibit acute toxicity toward aquatic organisms, even when the parent compound is removed [42].

Therefore, additional analyses such as total organic carbon (TOC), identification of intermediates using LC–MS, and ecotoxicity assays are recommended to ensure complete mineralization.

Furthermore, the potential leaching of Fe^{3+} and Zn^{2+} ions during repeated photocatalytic cycles should be evaluated to assess the long-term environmental safety of the catalyst. These considerations are essential for future real-world implementation.

3.7. Reusability of the Catalyst

Evaluating the reusability of a photocatalyst is crucial for ensuring environmental sustainability and cost-effectiveness in photocatalytic degradation processes. To examine the cyclic stability of the synthesized catalyst, the material was separated from the reaction mixture after each photocatalytic degradation run of atenolol. The recovered catalyst was then washed thoroughly with distilled water and dried in an oven at 60 °C before being reused in the subsequent cycle.

As shown in Table 5, the α-Fe_2O_3/ZnO/CP photocatalyst can be reused for up to five consecutive cycles without any significant loss in photocatalytic activity.

Beyond the fifth cycle, a gradual decline in removal efficiency becomes noticeable, which may be attributed to partial surface fouling, blockage of active sites, or slight reductions in charge-carrier mobility.

Table 4. The comparison of the prepared photocatalyst with other photocatalysts

	Drug	Photocatalyst	Degradation Removal (%)	Degradation Time	Ref.
1	ATL	Fe-TiO_2-Ag-ZnO	>63	98min.	[34]
2	ATL	TiO_2	78>	100 min.	[35]
3	ATL	Graphene TiO_2 composite	72	60 min.	[36]
4	ATL	TiO_2/Salicylaldehyde-NH_2-MIL-101(Cr)	60	60 min.	[37]
5	ATL	Y-Ag_3PO_4/CQDs/$BiVO_4$	90.9	6 h.	[38]
6	ATL	Ag-ZnO NPs	90.8	120 min.	[39]
7	ATL	rGO/$CuFe_2O_4$/CdS/Bi_2S_3QDs	76.5	360 min.	[40]
8	ATL	Fe-TiO_2	85	105 min.	[41]
9	ATL	α-Fe_2O_3-ZnO/CP	95.83	75min.	This work

Table 5. Reusability of α-Fe_2O_3/ZnO/CP for the photocatalytic degradation of atenolol

Cycle	R% ± SD[a]
1	96.85 ± 1.92
2	96.12 ± 1.98
3	95.04 ± 2.05
4	93.58 ± 2.14
5	92.21 ± 2.27
6	87.43 ± 2.39
7	82.16 ± 2.61

[a] Standard deviation

4. Conclusion

The α-Fe_2O_3/ZnO/CP nanocomposite was successfully synthesized, with structural characterization confirming the uniform distribution of spherical α-Fe_2O_3 and rod-like ZnO nanoparticles on the CP support, leading to enhanced photocatalytic efficiency and ease of separation. The Full-Factorial Design of Experiments provided a statistically valid and reliable model (supported by p-values and Confidence Intervals**)** that identified the crucial direct and interactive effects of the five process variables. The optimal degradation efficiency for Atenolol (ATL) was achieved under conditions of pH=9, low initial ATL concentration (10 mgL^{-1}), high H_2O_2 concentration (4 mgL^{-1}), catalyst composition of 75% Fe / 25% Zn and reaction time 75min. Building directly upon these optimized results, future research must focus on three critical areas for advancement.

Firstly, the long-term operational stability and reusability of the α-Fe_2O_3/ZnO/CP composite need rigorous validation through extensive cycling tests, especially before application in real wastewater.

Secondly, a deeper mechanistic understanding is required, specifically through radical scavenging experiments, to definitively identify the key reactive oxygen species driving the ATL degradation pathway.

Finally, to ensure environmental safety and efficacy, efforts should be directed toward exploring morphological engineering of the nanoparticles and conducting a comprehensive toxicological assessment of the treated effluent.

Future research should focus on evaluating the operational stability of the photocatalyst through multi-cycle degradation experiments under different environmental conditions, including variations in pH, ionic strength, and the presence of natural organic matter. It is also recommended to quantify metal leaching using ICP-OES and to perform XRD, SEM, and FTIR analyses after each cycle to monitor structural changes. Additionally, radical scavenging experiments could be employed to identify the dominant reactive species responsible for degradation. Testing the catalyst in real pharmaceutical wastewater will further clarify its practical applicability and performance in complex matrices.

Acknowledgements

The authors express their appreciation to the Research Council of Islamic Azad University of Mashhad, Iran for financial support.

Authors Contribution
All the authors have participated sufficiently in the intellectual content, conception and design of this work or the analysis and interpretation of the data (when applicable), as well as the writing of the manuscript.

Data availability
All data generated or analyzed during this study are included in this published article.

Conflict of interests
The author states that there is no conflict of interest.

References

[1] Majumdar A, Pal A. Clean Technol Environ Policy. 2020; 22:11 https://doi.org/10.1007/s10098-019-01766-1

[2] Bhatia V, Malekshoar Gh, Dhir A, Ray AK. J Photochem Photobiol A. 2017; 332:182. https://doi.org/10.1016/j.jphotochem.2016.08.029

[3] El-Salamony RA, Amdeha E, El Shafey AM, Al Sabagh AM. Int J Environ Anal Chem. 2023;103:868. https://doi.org/10.1080/03067319.2020.1865328

[4] Píštková V, Tasbihi M, Vávrová M, Štangar UL. J Photochem Photobiol A. 2015; 305:19. https://doi.org/10.1016/j.jphotochem.2015.02.014

[5] Ran Z, Wang L, Fang Y, Ma C, Li Sh. Catalysts. 2019; 9:876. https://doi.org/10.3390/catal9110876

[6] Leyva E, Moctezuma E, López M, Baines KM, Zermeño B. Catal Today. 2019; 323:14. https://doi.org/10.1016/j.cattod.2018.08.007

[7] Nosuhi M, Nezamzadeh-Ejhieh A. J Colloid Interface Sci. 2017;497:66. https://doi.org/10.1016/j.jcis.2017.02.055

[8] Saghi M, Mahanpoor K. Int J Ind Chem. 2017;8:297. https://doi.org/10.1007/s40090-016-0108-6

[9] Derikvandi H, Nezamzadeh-Ejhieh A. J Hazard Mater. 2017; 321:629. https://doi.org/10.1016/j.jhazmat.2016.09.056

[10] Majumder S, Chatterjee S, Basnet P, Mukherjee J. Environ Nanotechnol Monit Manag. 2020; 14:100386. https://doi.org/10.1016/j.enmm.2020.100386

[11] Chankhanittha T, Komchoo N, Senasu T, Piriyanon J, Youngme S, Hemavibool K, Nanan S. Colloids Surf A Physicochem Eng Asp. 2021; 626:127034.

https://doi.org/10.1016/j.colsurfa.2021.127034

[12] Davari N, Farhadian M, Solaimany Nazar AR, Homayoonfal M. J Environ Chem Eng. 2017;5:5707. https://doi.org/10.1016/j.jece.2017.10.052

[13] Mehrabadi Z, Faghihian H. J Photochem Photobiol A. 2018;356:102. https://doi.org/10.1016/J.JPHOTOCHEM.2017.12.042

[14] Tamiji T, Nezamzadeh-Ejhieh A. J Solid State Electrochem. 2019; 23:143. https://doi.org/10.1007/s10008-018-4119-4

[15] Shenoy S, Ahmed S, Lo IMC, Singh S, Sridharan K. Mater Res Bull. 2021; 140:111290. https://doi.org/10.1016/j.materresbull.2021.111290

[16] Kumar A, Khan M, Zeng X, Lo IMC. Chem Eng J. 2018; 353:645. https://doi.org/10.1016/j.cej.2018.07.153

[17] Wetchakun N, Wetchakun K, Sakulsermsuk S. Int J Ind Chem. 2020;11:161. https://doi.org/10.1007/s40090-020-00214-0

[18] Tatarchuk T, Danyliuk N, Shyichuk A, Macyk W, Naushad M. J Mol Liq. 2021;342:117407. https://doi.org/10.1016/j.molliq.2021.117407

[19] Jafarinejad A, Bashiri H, Salavati-Niasari M. Arab J Chem. 2022;15:104007. https://doi.org/10.1016/j.arabjc.2022.104007

[20] Liu W, Wang S, Wang J, Zhang B, Liu L, Liu H, Yang J. Ceram Int. 2022;48:22629. https://doi.org/10.1016/j.ceramint.2022.05.094

[21] Blourfrosh SK, Mahanpoor K. Int J Nano Dimens. 2021; 12:113. https://doi.org/10.22034/ijnd.2021.678595

[22] Sarabyar S, Farahbakhsh A, Tahmasebi HA, Mahmoodzadeh Vaziri B, Khosroyar S. Sci Rep. 2024;14:27390. https://doi.org/10.1038/s41598-024-73888-6

[23] Salesi S, Nezamzadeh-Ejhieh A. Environ Sci Pollut Res. 2023;30:105440. https://doi.org/10.1007/s11356-023-29730-z

[24] Noruozi A, Nezamzadeh-Ejhieh A. Chem Phys Lett. 2020; 752:137587. https://doi.org/10.1016/j.cplett.2020.137587

[25] Bharathi S, Nataraj D, Senthil K, Yoshitake M. J Nanopart Res. 2013;15:113. https://doi.org/10.1007/978-3-319-05041-6_9

[26] Getie S, Belay A, Chandra Reddy AR, Belay Z. J Nanomed Nanotechnol. 2017; S8. https://doi.org/10.4172/2157-7439.S8-004

[27] Pan Y, Zhang Y, Huang Y, Jia Y, Chen L, Cui H. J Alloys Compd. 2022;926:166848. https://doi.org/10.1016/j.jallcom.2022.166848

[28] Yousefi Q, Nezamzadeh-Ejhieh A. Solid State Sci. 2024;154:107584. https://doi.org/10.1016/j.solidstatesciences.2024.107584

[29] Sharafzadeh S, Zolgharnein J, Nezamzadeh-Ejhieh A, Dermanaki Farahani S. Int J Hydrog Energy. 2025; 106:1429. https://doi.org/10.1016/j.ijhydene.2025.02.031

[30] Abdullah TA, Al-Obaidi Q, Abdulla TA, Rasheed RT, Al-Azawi K, Meharban F. Hung J Ind Chem. 2023;51:65. https://doi.org/10.33927/hjic-2023-20

[31] Abu-Dief AM, Mohamed WS. Curr Catal. 2020; 9:128. https://doi.org/10.2174/2211544709999201123193710

[32] Rezaei M, Nezamzadeh-Ejhieh A, Massah A. Energy Fuels. 2024; 38:7637. https://doi.org/10.1021/acs.energyfuels.4c00325

[33] Mirsalari SA, Nezamzadeh-Ejhieh A, Massah A. Environ Sci Pollut Res. 2022;29:33013. https://doi.org/10.1007/s11356-021-17569-1

[34] Omrani N, Nezamzadeh-Ejhieh A. Int J Hydrog Energy. 2020:19144. https://doi.org/10.1016/j.ijhydene.2020.05.019

[35] Ramasamy B, Jeyanthi J, Chinnaiyan P. Environ Nanotechnol Monit Manag. 22023; 19:100779 https://doi.org/10.1016/j.enmm.2023.100779

[36] Tammaro M, Fiandra V, Mascolo MC, Salluzzo A, Riccio C, Lancia A. J Environ Chem Eng. 2017;5:3224. https://doi.org/10.1016/j.jece.2017.06.026

[37] Bhatia V, Malekshoar G, Dhir A, Ray AK. J Photochem Photobiol A. 2017; 332:182. https://doi.org/10.1016/j.jphotochem.2016.08.029

[38] Mehrabadi Z, Faghihian H. J Photochem Photobiol A. 2018;356:102. https://doi.org/10.1016/j.jphotochem.2017.12.042

[39] Wang Y, Niu J, Gao X, Zhang Y. Appl Surf Sci. 2020;533:147458. https://doi.org/10.1016/j.apsusc.2020.1474

[40] Ramasamy B, Jeyadharmarajan J, Chinnaiyan P. Environ Sci Pollut Res. 2021;28:39637. https://doi.org/10.1016/j.rechem.2023.101200

[41] Rajeshwari MR, Syed A, Bahkali AH, Elgorban AM, Rahiman MK, Varma RS, Khan SS. J Ind Eng Chem. 2022;115:402. https://doi.org/10.1016/j.jiec.2022.08.024

[42] Bhuvaneswari R, Jeyanthi J, Kumar M. Opt Mater X. 2021;239:166658. https://doi.org/10.1016/j.omx.2022.100178

[43] Kanakaraju D, Glass BD, Goh PS. Environ Sci Pollut Res. 2025;32:14316. https://doi.org/10.1007/s11356-025-36547-5

2228-5970 [https://doi.org/10.57647/j.ijic.2025.1604.15]